Review

Author for correspondence:
Laura Schaefer
e-mail: lschaefer@asu.edu

Magma oceans as a critical stage in the tectonic development of rocky planets

Laura Schaefer and Linda T. Elkins-Tanton

School of Earth and Space Exploration, Arizona State University, Tempe, AZ 85287, USA

LS, 0000-0003-2915-5025; LTE-T, 0000-0003-4008-1098

Magma oceans are a common result of the high degree of heating that occurs during planet formation. It is thought that almost all of the large rocky bodies in the Solar System went through at least one magma ocean phase. In this paper, we review some of the ways in which magma ocean models for the Earth, Moon and Mars match present-day observations of mantle reservoirs, internal structure and primordial crusts, and then we present new calculations for the oxidation state of the mantle produced during the magma ocean phase. The crystallization of magma oceans probably leads to a massive mantle overturn that may set up a stably stratified mantle. This may lead to significant delays or total prevention of plate tectonics on some planets. We review recent models that may help alleviate the mantle stability issue and lead to earlier onset of plate tectonics.

This article is part of a discussion meeting issue 'Earth dynamics and the development of plate tectonics'.

1. Magma oceans are common

Magma oceans appear to be a common outcome of formation processes for large rocky bodies [1,2]. Small planetesimals and embryos can form on very short time scales in the protoplanetary disc, so that they incorporate significant amounts of short-lived radionuclides such as ^{26}Al and ^{60}Fe that can produce enough heat to at least partially melt many of these objects [3,4]. Models suggest that the asteroid 4 Vesta, which is the source of the howardite–eucrite–diogenite (HED) meteorites, went through a magma ocean stage due to such short-lived heating [5–7]. Many iron meteorites, which are probably the remnants of differentiated planetesimals, have ages of only

approximately 1 Myr after Solar System formation, indicating very early, short-lived magma oceans [8,9]. Larger objects like the Earth take long enough to assemble that short-lived radionuclides cannot provide sufficient heating to melt them. For these larger, later-assembling bodies, substantial heating can come from accretionary impacts (e.g. [10,11]) and gravitational segregation of metallic iron into the centre of the planet. Giant impacts also appear to be common in N-body simulations of rocky planet formation [12], and are likely to cause widespread melting that can lead to differentiation in both silicates and metals [13].

In this paper, we will discuss several ways in which forward magma ocean models do a good job of matching real-world observations of the Earth, Moon and Mars. Magma ocean models can produce large, low-shear velocity provinces (LLSVPs) at the base of Earth's mantle through cumulate overturn and predict that these structures are stable over billions of years. Lunar magma ocean models can produce the internal differentiation of the Moon, including the anorthositic crust, the source regions for the picritic glasses and mare basalts, and the KREEP component, rich in incompatible elements. Models of the magma ocean on Mars can produce early crust, some of which may be preserved to the present day, and which could be hydrated by the earliest atmosphere to produce primordial clays. We also introduce new calculations that show that magma ocean models can produce the present-day mantle oxidation state of the Earth through metal–silicate equilibration within the magma ocean, with no additional mechanisms required. We will then discuss the mantle state at the end of the magma ocean period and discuss whether it can hinder or allow early onset of plate tectonics.

2. Magma ocean models match observations

Magma ocean models have been applied to all of the terrestrial planets, as well as the Earth's Moon. These models match observable properties of the present-day planets. The case for magma oceans on the Moon and Mars are easier to make because of the lack of active tectonic processing over most of the Solar System history. For the Earth, models can match deep mantle structures and the chemical properties of the mantle, including the abundances of trace elements and the present-day oxidation state. We review these model predictions below and present new calculations of the oxidation state of the magma ocean during core formation on the Earth.

(a) Differentiation of the lunar interior

Magma ocean models were first fully developed to explain observations and measurements of Apollo-returned samples from the Moon indicating that there was abundant plagioclase feldspar in the lunar crust [14–16]. The feldspar found in the lunar crust is nearly pure (greater than 98%) anorthosite, containing trace amounts of mafic phases [15,17,18]. Lunar meteorites, remote spectroscopy and gravity field studies all support the widespread distribution of anorthosite in the lunar crust [19–21]. This widespread occurrence has led to the hypothesis that the Moon was at least partially molten and that anorthite plagioclase buoyantly segregated from the melt to form the crust [14–16]. This early silicate differentiation event is widely believed to have been a lunar magma ocean, which would be a natural consequence of the Moon-forming impact. In addition to the anorthositic crust, the existence of the highly incompatible element-enriched KREEP (K, Rare Earth Element and P-rich) component, as well as the positive Eu anomalies in the highlands anorthosites and complementary negative Eu anomalies in mare basalts (e.g. [22–24]) provide additional evidence in favour of a global lunar magma ocean. Models of metal–silicate partitioning during lunar core formation are also consistent with equilibration occurring at the lunar core-mantle boundary (CMB), indicating a fully molten Moon [25].

Numerous authors have modelled the crystallization of the lunar magma ocean (e.g. [13,26–33]). The lunar magma ocean would initially be fully molten at the surface and could rapidly cool and solidify by approximately 80% by volume in the first 1 ky [33]. The first solids would include Mg-rich olivine followed by orthopyroxene in the lower lunar mantle. Above 70–80% solidification, plagioclase begins to crystallize, and because it is lower in density than the

magma ocean liquid, it should have floated to the surface to form a thermally conductive lid. Expulsion of trapped liquid by compaction and other processes would limit the amount of mafic minerals that could have formed in the crust, in agreement with observations (e.g. [34,35]). The magma ocean melt becomes more Fe-rich as crystallization proceeds, with a very dense ilmenite-bearing layer forming after about 95% crystallization. The residual liquids are very enriched in incompatible elements and have compositional characteristics similar to those found in the KREEP component [30]. Thermal models show that the conductive anorthositic crust (approx. 40–50 km) would have delayed the solidification of the remaining magma ocean by approximately 10 Myr [33]. However, ages for lunar crustal materials, discussed below, suggest that magma ocean crystallization was not complete until approximately 150–200 Myr. Recent models have shown, however, that tidal heating may extend the crystallization of this final magma ocean liquid out to 200 Myr [36,37]. Gravitationally driven cumulate overturn could produce later episodes of volcanism that would explain the ages and compositions of the Mg-suite of lunar crustal rocks [33].

Magma ocean crystallization experiments [32,38,39] reproduce many aspects of the numerical magma ocean models, including increasing density of the cumulates with crystallization, but some discrepancies remain. In particular, although liquid evolution trends are broadly similar between experiments and models, the late-stage liquid composition can differ significantly (Gaffney *et al*. [40]). Recent experiments suggest that a dry lunar magma ocean would produce much thicker anorthositic crust than observed by the GRAIL mission, but a wet lunar magma ocean containing 270–1650 ppm of water would produce a thinner crust [38,39]. This water abundance is consistent with recent measurements of water abundances in lunar anorthosites [41]. Additional models including the effect of water on the crystallization time will be needed to compare with lunar geochronology measurements discussed below in order to confirm a wet lunar magma ocean.

The age of lunar crustal anorthosites provides a constraint on the crystallization age of the lunar magma ocean, but measured ages cover a large span, from 4.47 to 4.29 Gyr (e.g. [42–47]). Kleine *et al*. [48] reviewed the isotopic ages for lunar samples available at the time and concluded that the combined constraints from the Hf-W and ^{147}Sm-^{143}Nd systems indicated that the lunar magma ocean reached approximately 70% crystallization, at which point anorthosite flotation should begin, no earlier than 60 Myr and no later than 150 Myr. Borg *et al*. [49] reported a very young age of crystallization of a ferroan anorthosite of 4360 ± 3 million years from the combined analysis of the ^{207}Pb-^{206}Pb, ^{147}Sm-^{143}Nd and ^{146}Sm-^{142}Nd isotopic systems, making this the most reliable FAN age, and suggested that the lunar crust was produced by non-magma ocean processes such as serial magmatism. Boyet *et al*. [50] measured Sm-Nd systematics in several lunar ferroan anorthosite samples and found that they did not form a single isochron, which the authors suggest indicates that all but one of these samples formed through later magmatism or processing after the lunar magma ocean crystallization. The one sample with the largest deficit in ^{142}Nd gave a crystallization age of 60–125 Myr after Solar System formation for lunar crust formation. Recent results from Pb-isotopic evolution in lunar basalts have suggested a large differentiation event at 4376 ± 18 Myr, which could coincide with the last stages of lunar magma ocean crystallization [51], consistent with the 142Nd ages for FAN 60025 [49]. Ages determined for lunar zircons indicate a younger age of 4.51 Gyr for lunar crustal formation [52], which is significantly older than ages from ferroan anorthosites. This age, which is closer to Moon-formation ages of approximately 60 Myr from Hf-W [48], may instead simply represent the time of zircon formation in the initially rapidly cooling lunar magma ocean [53]. Modelling by Meyer *et al*. [36] suggests that prolonged cooling of the crust due to tidal heating could explain the late ages determined for the lunar anorthosites relative to the much shorter expected cooling times (e.g. [33]).

One significant observation that cannot readily be explained by lunar serial magmatism, and therefore requires a deep magma ocean, is the apparent ubiquity of an orthopyroxene + olivine melting source region for the picritic glasses between approximately 250 and approximately 500 km depth on the lunar nearside (data summary in [33], fig. 6). This thick deep layer of uniform

mineralogy must have been created by a deep, fractionating magma ocean: serial diapirs will not leave behind a uniform cumulate pile, and the heterogeneities from between the putative melting regions would be enriched and therefore melt at lower temperatures later, producing melt products different from the picritic glasses, and not sampled on the Moon.

Further, the lunar crust's thickness is smoothly varying from the nearside to the far side, excepting the effects of large impacts. To produce a smoothly varying crustal thickness via serial magmatism, the wavelength of the diapirs must not be more than a few multiples of the crustal thickness, or relaxation of the rapidly cooling and high-viscosity anorthosites would not produce a smoothly varying crustal thickness. Such ubiquity of melting around the Moon must be virtually indistinguishable from a global magma ocean.

Many aspects of the lunar magma ocean remain to be investigated, including the depth of the magma ocean, partial equilibrium versus fully fractional crystallization [30,33], the cooling times of the crust and the possible formation of a crustal dichotomy between nearside and far side of the Moon [54,55]. While many details of the chronology of lunar geology remain to be explained, the lunar magma ocean model is very successful in producing many of the observed properties of the Moon's internal structure and surface composition.

(b) Martian crust and clay formation

An early Martian magma ocean is supported by measurements of short-lived radioactive isotopes that indicate early differentiation of Mars and generation of enriched and depleted mantle reservoirs [9,56–58]. Young core formation ages for Mars (greater than approx. 4–10 Myr) [59] are further argument for a magma ocean, because short-lived radioactive isotopes such as ^{26}Al would still have been present to provide additional heat and core segregation requires at least partial melting of the silicate mantle. However, it remains uncertain how deep the magma ocean on Mars would have been. Physical models of the accretion and differentiation of Mars have attempted to determine the degree of melting with variable results. Models using impact heating and cooling but no other heat source find only partial melting of the near surface and a cold interior [60]. A multiphase model including radioactive and gravitational heating found that core formation may be a catastrophic, early event that can lead to additional heating of Mars-sized objects, although full silicate melting is not required [61]. The blanketing effect of a hybrid proto-atmosphere (both outgassed and nebular components) could also help to sustain a global magma ocean throughout accretion, depending on the accretion rate of proto-Mars [62]. No model including all of the physical processes controlling the heating and cooling of proto-Mars (impact heating and cooling, radioactive decay, atmospheric blanketing, gravitational segregation, thermal convection, etc.) exists, and the physical partitioning of energy of those processes remains largely unknown, so the depth of the Martian magma ocean remains uncertain.

The magma ocean stage may have produced silicate reservoirs enriched and depleted in incompatible elements during fractional crystallization, which remain today due to incomplete mantle mixing. The ages of these reservoirs as measured with short-lived radioactive isotope systems have been used to infer the duration of the magma ocean stage and timing of crust formation, although interpretations within the community can vary. Measurements of Sm-Nd isotope systematics in shergottites by Debaille *et al.* [63] suggest that the magma ocean stage on Mars lasted for approximately 100 Myr, with a depleted reservoir forming by 4.535 Gyr and an enriched reservoir, plausibly either the crust of late-stage magma ocean liquids, forming by 4.457 Myr. Lead–lead ages of zircons in the polymict breccia NWA 7034/7355, which formed through melting of primary crust, give maximum crustal formation times of 4.428 Gyr [64]. Whole-rock Sm-Nd ages of the same meteorite give similar ages of 4.42–4.46 Gyr [65]. Coexisting variations of ε^{182}W and ε^{142}Nd have been attributed to multiple episodes of silicate differentiation [9]. These authors find formation times of the depleted reservoir of approximately 25 Myr, with ongoing formation of the enriched reservoir (thought to be the crust), extending to at least 40 Myr after Solar System formation. This is approximately 60 Myr younger than in [63] and approximately 100 Myr younger than in [64,65] but is more consistent with results from Martian

crust formation models [66]. In comparison, magma ocean thermal models predict crystallization time scales less than 5 Myr for Mars [67,68]. Additional analyses of Sm-Nd isotope systematics in shergottites and nahklites found a silicate differentiation time of 4504 Myr (approx. 60 Myr after Solar System formation) [69]. Given the discrepancy with magma ocean thermal models [67,68], these authors suggest that this age could be explained by a giant impact and heterogeneous mixing of the Martian mantle, rather than a global silicate differentiation event. However, recent high-precision isotopic work on zircons by Bouvier *et al.* [58] shows that the Martian magma ocean was solidified in less than 10 Myr after planetary formation, a result that indicates that a solid Mars existed within 20 Myr of calcium–aluminum-rich inclusions. This result supports the rapid solidification of the Martian magma ocean and indicates that later reservoir disruptions were probably due to giant impacts and remixing.

Elkins-Tanton *et al.* [66] modelled early crust formation on Mars at 30–50 Myr after accretion arising during cumulate overturn by melting of the hot cumulates rising into the upper mantle. Measurements of potentially ancient crust in crater central peaks find primarily dunite and pyroxenite-dominated lithologies. Compositional variations are suggestive of high degrees of fractional crystallization in a slowly cooling magma body, potentially generated by the overturn of the mantle following magma ocean solidification [70]. However, Plesa *et al.* [71] find that stagnant lid convection models beginning from a thermal and density state derived from fractional crystallization cannot reproduce the later long-term thermal evolution of the planet (e.g. 1–2 long-lived mantle plumes). Therefore, more work is still needed in understanding the depth and longevity of the Martian magma ocean, and the post-overturn thermal state.

Clays are relatively common on the surface of Mars [72], suggesting the widespread presence of water on the surface (or near-surface) throughout the Noachian. Their presence has been used to try to constrain the climate history of early Mars, with models ranging from 'warm and wet' to 'cold and transiently wet' [73,74]. However, magma ocean models provide another possible source for clay minerals. Magma ocean outgassing would result in a thick atmosphere, of which a large or primary component is water vapour (e.g. [67]). Primitive clays found on the surface of Mars could have formed through rapid reaction of a supercritical steam atmosphere or hot early ocean during the late magma ocean stage with the earliest magma ocean crust [75]. Although this clay layer would later be buried by a new crust [67], this model may account for the presence of a thick clay layer at large depths within the Martian crust observed in crater central peaks [76] and the abundance of clay minerals within the regolith. The clay formation model assumes the long-term stability of the crust against the overturn, which should be further investigated. Early clays would probably have lower D/H ratios, because they would have formed before significant water escape from the planet, which provides a testable prediction of the primordial clay model.

(c) Chemical heterogeneities in the Earth's lower mantle

Seismic studies have long noted large-scale heterogeneities in the lower mantle from variations in seismic velocities [77,78]. Both seismically fast and slow regions have been identified. While the seismically fast regions seem to be associated with regions of subduction, the seismically slow regions—called large LLSVPs—are found in regions associated with hot spot volcanism [79,80]. Seismic tomography suggests that the LLSVPs are associated with chemical heterogeneity in the lower mantle, and that these regions have higher densities than the surrounding lower mantle [81,82]. Within the LLSVPs are small (5–40 km thick) regions of even lower seismic velocity (ultralow-velocity zones, ULVZs) that have been associated with partial melting of silicates directly above the core or with significant compositional differences [83–86]. Geodynamics simulations suggest that the LLSVPs could have been stable throughout Earth's history if they are higher in density and/or viscosity than the surrounding lower mantle [87–89], suggesting a potential primordial origin.

Chemical heterogeneities within the mantle suggest the existence of a small enriched mantle reservoir in the deep mantle [44,90]. This suggestion is based on the Earth's $^{142}Nd/^{144}Nd$ ratio, which is higher than measured in chondrites and suggests that an early silicate differentiation

event occurred in the first 160 Myr [91]. Other recent measurements [92] suggest that the Earth has the same $^{142}Nd/^{144}Nd$ ratio as enstatite chondrites, obviating the need for an enriched reservoir. Other arguments in favour of a primordial chemical reservoir in the mantle come from noble gases. Mid-ocean ridge basalts (MORBs) and ocean island basalts (OIBs) appear to tap different chemical reservoirs, with the MORB source being depleted in primordial noble gas components and the OIB source being enriched and potentially undegassed [93–97].

Fractional crystallization of a magma ocean produces an unstable density stratification due to the enrichment of Fe in late-stage melts [1,67,98–100]. These models predict mantle overturn following the crystallization of the magma ocean, with the final iron-rich residues sinking to the CMB of the planet. As they are denser than the overlying mantle, these overturned cumulates might be stable at the CMB on long time scales (e.g. [101]), so models suggest that these could be responsible for the modern-day LLSVPs [102].

Alternative primordial origins for the LLSVPs have been suggested, including a primary basal magma ocean [103], partial melting of the Archaean mantle and sinking of dense, Fe-rich melts [104], or subduction of early crust enriched with late delivered chondritic material [94,105]. A primary basal magma ocean is produced if the liquidus and the magma ocean adiabat first intersect in the middle of the mantle, with crystallization proceeding towards the surface rapidly, and more slowly towards the core. The basalt melt would represent an undepleted primordial chemical reservoir, which could generate denser crystallization products as Fe becomes enriched in the melt [103]. Zhang *et al*. [106] alter the basal magma ocean model to suggest that the higher density of the LLSVPs is due to the trapping of Fe-Ni-S metallic liquids within the basal magma ocean cumulates. However, recent analysis of the mantle melting curve [107] suggests the mantle liquidus should increase smoothly from the surface to the CMB. If this is verified by further experiments, magma ocean crystallization would initiate at the CMB, and a primary basal magma ocean could probably be ruled out.

(d) Mantle oxidation state

The oxidation state of the upper mantle of the present-day Earth is near the FMQ buffer [108]. Various estimates of the mantle redox state through time are shown in figure 1. Measurements of ancient redox proxies, Cr and V whole-rock abundances in ancient volcanics, and the composition of Cr-rich spinels in ancient volcanics indicate that the oxygen fugacity of the mantle has been at or above the present-day value ($\pm 0.5 \log fO_2$) since approximately 3900 Ma [109]. Canil [110] used partitioning of V between komatiitic liquids and olivine in 6 well-characterized komatiite flows to estimate Archaean fO_2 and found values from ΔNNO −2 to +1. Li & Lee [111] looked at V/Sc ratios in basalts and find that Archaean basalts have V/Sc ratios only slightly smaller than that of modern MORBS, indicating only a minor decrease of approximately $0.3 \log fO_2$ units relative to FMQ. Recent measurements of 3.5–2.4 Ga komatiites used V partitioning behaviour to constrain the fO_2 of the mantle, and found a range of −0.11 to +0.43 FMQ, consistent with a relatively constant mantle fO_2 through time [112]. Aulbach & Stagno [113] used V/Sc ratios in metamorphosed mid-MORBs and picrites from 3.0 to 0.55 Ga as redox proxies and found a slightly larger decrease in mantle fO_2, down to −1.5 FMQ, during the Archean. They note that the increase of the mantle fO_2 to the present-day value appears coincident with the atmospheric great oxidation event (GOE). Analysis of Ce abundances in detrital Hadean-aged Jack Hills zircons suggest oxygen fugacities back to 4.3 Ga consistent with those of the present day [114]. Taken together, the present measurements are consistent with a constant oxygen fugacity within the mantle over the entire history of the Earth.

However, models of core formation, which occurs within the magma ocean of the forming Earth, require much more reducing conditions in order to match trace element partitioning behaviour between the mantle and the core (e.g. [115–117]). Therefore, oxidation of the mantle to the present-day state had to occur contemporaneously with core formation or shortly thereafter and operate on a relatively short time scale. Several models have been proposed to increase the oxidation state of the mantle through the post-production of Fe^{3+} in the mantle. These
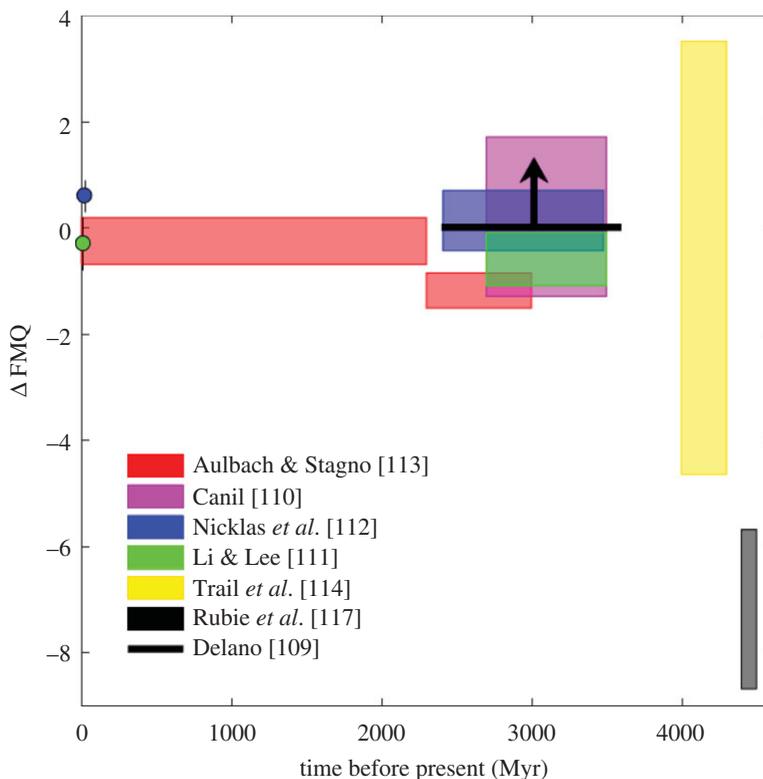
Figure 1. Oxidation state of Earth's mantle through geologic time from redox proxy measurements. See text for source details. The two data points at approximately 0 Myr are values for present-day MORBs. We plot historical oxygen fugacity relative to the fayalite–magnetite–quartz buffer (FMQ). At 1200C and 1 GPa, NNO = FMQ + 0.7, IW = FMQ − 3.69.

include gradual H escape from accreted water [118], and the production of Fe^{3+} through disproportionation of Fe^{2+} in the lower mantle by crystallization of bridgmanite [119,120]. Trace element partitioning models (e.g. [117,121]) match the present-day mantle FeO abundance by allowing the composition of accreting material to become more oxidized through time (IW-5 to IW-2), but these models fail to predict $Fe^{3+}/\Sigma Fe$, which governs the present-day oxidation state. These models typically end with a mantle at IW-2, about 5 log fO_2 units below the present day.

We propose an alternative mechanism: that disproportionation of Fe^{2+} occurs in the silicate melt phase in the magma ocean during equilibration with the core-forming metal delivered by accreting impactors, rather than during crystallization. This allows immediate separation of the metallic liquid, avoiding the remixing problem of [119,120]. The equilibrium among the different Fe valence states will be given by the reaction 3FeO(melt) -greater than $2FeO_{1.5}$(melt) + Fe (liquid metal). The metal will sink through the magma ocean to join the core, leaving the oxidized mantle material behind, without requiring complicated scenarios of melting and recrystallizing of bridgmanite that would be difficult to quantify. To reproduce the present-day upper mantle, metal–silicate equilibration in the melt at high pressures must produce $Fe^{3+}/\Sigma Fe \sim 0.01$–$0.05$ [108]. As in [122], we assume that equilibrium will be controlled at the level of metal–silicate equilibration and the magma ocean composition would be rapidly homogenized by convection. In figure 2, we show the amount of Fe^{3+} produced through this reaction as a function of temperature along the mantle liquidus [123], using different datasets for partial molar volumes of the molten iron oxides [124,125]. The low-pressure model data [124,126] were measured at 1 bar, whereas for the higher-pressure model, we use data from new measurements of the $Fe^{3+}/\Sigma Fe$ ratio in high-pressure melts [125] of up to 7 GPa to refit the partial molar volume of the Fe^{3+}
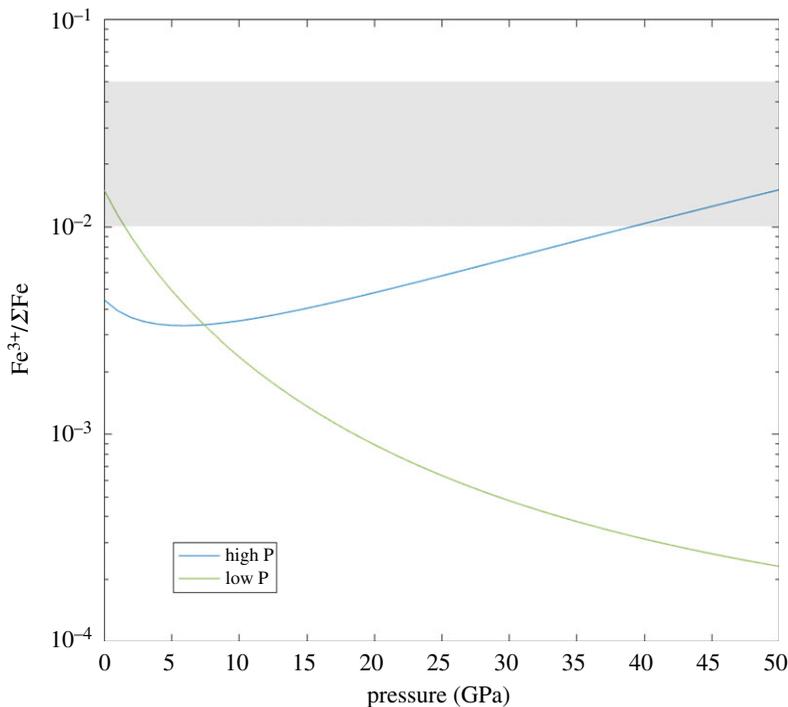
Figure 2. $Fe^{3+}/\Sigma Fe$ in the magma ocean produced by equilibration of liquid silicate and core-forming metal as a function of pressure along the mantle liquidus of [123]. Table 1 gives thermodynamic data sources. The grey-shaded region highlights the $Fe^{3+}/\Sigma Fe$ values in the Earth's present-day upper mantle [108]. (Online version in colour.)

Table 1. Fit parameters used to calculate the $Fe^{3+}/\Sigma Fe$ ratio as a function of pressure (figure 2). We refit the data of [125] to a Murnaghan equation of state for $FeO_{1.5}$ (liq), while taking values from Lange *et al.* [124] and Kress & Carmicheal [126] for FeO(liq). For both models, we take the standard Gibbs energy of formation of the liquid oxides from Kowalski & Spencer [129] and calculate activity coefficients for the liquid oxides from Matousek [130]. For both models, we take a value of $\kappa' = 4$ for both oxides.

	low P model	reference	high P model	reference
$\bar{V}_{FeO}$ (cm^3 mole^{-1})	13.65	[124]	13.65	[124]
$\bar{V}_{FeO1.5}$ (cm^3 mole^{-1})	21.065	[124]	18.9	fit to [125]
κ_{FeO} (GPa)	30.33	[126]	30.33	[126]
$\kappa_{FeO_{1.5}}$ (GPa)	16.6	[126]	10.8	fit to [125]

oxide. We use the equation of state of liquid Fe metal from Komabayashi [127] for all calculations and include partitioning of oxygen and silicon into the metal phase using the partitioning model of [128]. The thermodynamic data used for these calculations are given in table 1. We calculate the $Fe^{3+}/\Sigma Fe$ ratio as a function of pressure up to 50 GPa, which is close to average conditions of core formation determined for the Earth from trace element partitioning studies [117,121].

The updated equation of state for the liquid iron oxide from Zhang *et al.* [125] predicts much larger Fe^{3+} abundances would be produced at high pressures than the 1 bar data of [124] do. This is consistent with new, unpublished measurements of $Fe^{3+}/\Sigma Fe$ in silicate melts from Armstrong *et al.* [131], which go up to pressures of approximately 25 GPa. The stabilization of Fe^{3+} in the

melt phase at high pressure was predicted by Hirschmann [122], partially on the basis of the stability of Fe^{3+} in the crystalline phase at high pressures. As figure 2 shows, the equilibration of the different Fe valences at high pressure during the separation of core-forming metal can easily produce the observed present-day Fe^{3+} abundances in the Earth's upper mantle, shown by the grey-shaded region. Therefore, no additional oxidation mechanisms are required to produce the present-day oxidation state, which implies that there has been limited oxidation of the Earth's upper mantle over geologic time. The calculations with the new data also suggest that the mantles of larger planets should in general be more oxidized than smaller planets once the metallic phase has separated, given that more Fe^{3+} is produced at higher pressures. This is corroborated by the low initial oxygen fugacity of the depleted Martian mantle (approx. IW) [132], in comparison to the Earth's much higher oxygen fugacity. This has significant implications for the compositions of outgassed atmospheres we should expect on rocky exoplanets of different sizes.

3. Magma oceans set the initial conditions for planetary tectonics

(a) Density stratification and magma ocean overturn

Models of fractional crystallization of magma oceans result in unstable density structures due to the enrichment of late-stage melts in iron. These crystallization models predict whole-mantle overturn at the end of magma ocean crystallization, which results in a stably stratified density structure in the earliest solid mantle. This stable stratification is predicted to inhibit the onset of whole-mantle convection, which may result in an early stagnant lid tectonic regime on rocky planets [133,134]. Recent models [135,136] investigate the possibility of solid-state convection beginning within the cumulate pile before the magma ocean has fully crystallized. Ballmer *et al.* [135] investigate incremental overturns within the solidifying cumulate pile using 2D numerical convection simulations and find that the majority of the mantle becomes well mixed. However, the final Fe-rich cumulate melt layer sinks to the CMB during the final overturn and remains stable as a highly dense layer for geologic time, which may be related to present-day LLSVPs. Maurice *et al.* [136] similarly find that early onset of solid-state convection while the magma ocean is still crystallizing will more efficiently homogenize the mantle than late-stage overturn. However, their model fails to produce a LLSVP-like zone at the base of the mantle, and they instead prefer the basal magma ocean model of [103]. Tikoo & Elkins-Tanton [137] show that water within the late-stage melt may be expelled during mantle overturn, which would cause a large influx of water into the upper mantle. The large abundance of water in the early upper mantle would have allowed partial melting and lowered the viscosity, possibly allowing the early initiation of whole-mantle convection. These models show that the mantle structure at the end of magma ocean phases remains uncertain.

(b) Tectonics after the magma ocean

Recent work in scaling theory, steady-state simulations and numerical evolutionary models show that the initial conditions of a solid-state mantle convection simulation can strongly influence the tectonic style of the simulated planet [138–140]. For instance, the authors in [138] demonstrate that tectonic models show a history dependence, i.e. the tectonic mode of a system is determined by its specific geologic and climatic history. Therefore, the density and thermal structure at the end of the magma ocean stage and following cumulate overturn sets the stage for the future tectonic evolution of the planet. As discussed in the previous section, a number of parameters remain poorly constrained by the end stage of magma ocean models, which influences the later tectonic models. The uncertain parameters include the mantle potential temperature and heat flux, the degree of mantle hydration, the thickness of the lithosphere and the planetary climate.

After discovering remnant magnetism on Mars, models predicting early plate tectonics were popular to explain rapid core cooling needed for magnetic field generation [141]. However, evidence of significant mantle heterogeneities on Mars suggest that significant convective mixing

has not occurred. There is also little evidence of crustal recycling, indicating that Mars probably entered a stagnant- or sluggish-lid phase following the magma ocean [71,134], with heat fluxes out of the mantle dominated by a few long-lived mantle plumes.

It remains uncertain if plate tectonics on the Earth can initiate immediately after the magma ocean stage, or if the magma ocean is more likely to be followed by a stagnant-lid mode [142] or alternative tectonic regime (e.g. squishy lid [143], heat pipe model [144], etc.). Foley *et al.* [145] investigate onset of subduction during the Hadean using a model including grain damage and find that a period of stagnant lid convection follows the initial mantle overturn, and that sluggish subduction can initiate relatively rapidly, due to damage build-up in the cold, dense lid material. Recent models have highlighted the potential role of triggers for initiating subduction, including external impacts that punch through the lithosphere and mantle plumes [146,147]. Numerical models of core formation suggest that metal diapirs may set up conduits to permit early onset of mantle plumes, either purely thermal or thermochemically driven [148,149], which is particularly effective if the magma ocean is restricted to the upper mantle. These early mantle plumes could then play a role in triggering onset of early subduction.

This discussion highlights the uncertainty in the tectonic state of planets following the magma ocean stage and the need for additional modelling. Magma ocean models must in future be more coupled with petrologic data from short-lived isotopic systems to help us better understand the early evolution of the terrestrial planets and the requirements for the onset of plate tectonics. Plate tectonics is often thought to be essential for the sustainability of life, and therefore such work has implications for the search for life on exoplanets as well as in our own Solar System.

References

1. Solomatov V. 2000 Fluid dynamics of a terrestrial magma ocean. In *Origin of the earth and moon* (eds RM Canup, K Righter), pp. 323–338. Tucson, AZ: University AZ Press.
2. Elkins-Tanton LT. 2012 Magma oceans in the inner solar system. *Ann. Rev. Earth Planet. Sci.* **40**, 113–139. (doi:10.1146/annurev-earth-042711-105503)
3. Miyamoto M, Fujii N, Takeda H. 1981 Ordinary chondrite parent body: an internal heating model. *Proc. Lunar Planet. Sci. Conf.* **12**, 1145–1152.
4. Hevey PJ, Sanders IS. 2006 A model for planetesimal meltdown by ^{26}Al and its implications for meteorite parent bodies. *Met. Planet. Sci.* **41**, 95–106. (doi:10.1111/j.1945-5100.2006.tb00195.x)
5. Papanastassiou DA, Wasserburg GJ. 1969 Initial strontium isotopic abundances and the resolution of small time differences in the formation of planetary objects. *Earth Planet. Sci. Lett.* **5**, 361–376. (doi:10.1016/S0012-821X(68)80066-4)
6. Neumann W, Breuer D, Spohn T. 2014 Differentiation of Vesta: implications for a shallow magma ocean. *Earth Planet. Sci. Lett.* **395**, 267–280. (doi:10.1016/j.epsl.2014.03.033)
7. Mandler BE, Elkins-Tanton LT. 2013 The origin of eucrites, diogenites, and olivine diogenites: magma ocean crystallization and shallow magma chamber processes on Vesta. *Met. Planet. Sci.* **48**, 2333–2349. (doi:10.1111/maps.12135)
8. Scherstén A, Elliott T, Hawkesworth C, Russell S, Masarik J. 2006 Hf-W evidence for rapid differentiation of iron meteorite parent bodies. *Earth Planet. Sci. Lett.* **241**, 530–542. (doi:10.1016/j.epsl.2005.11.025)
9. Kruijer TS, Kleine T, Borg LE, Brennecka GA, Irving AJ, Bischoff A, Agee CB. 2017 The early differentiation of Mars inferred from Hf-W chronometry. *Earth Planet. Sci. Lett.* **474**, 345–354. (doi:10.1016/j.epsl.2017.06.047)

10. Matsui T, Abe Y. 1986 Formation of a 'magma ocean' on the terrestrial planets due to the blanketing effect of an impact-induced atmosphere. *Earth Moon Planets* **34**, 223–230. (doi:10.1007/BF00145081)

11. Abe Y. 2011 Protoatmospheres and surface environment of protoplanets. *Earth Moon Planets* **108**, 9–14. (doi:10.1007/s11038-010-9368-x)

12. Quintana EV, Barclay T, Borucki WJ, Rowe JF, Chambers JE. 2016 The frequency of giant impacts on Earth-like worlds. *Astrophys. J.* **821**, 126. (doi:10.3847/0004-637X/821/2/126)

13. Tonks WB, Melosh HJ. 1993 Magma ocean formation due to giant impacts. *J. Geophys. Res.* **98**, 5319–5333. (doi:10.1029/92JE02726)

14. Smith JV, Anderson AT, Newton RC, Olsen EJ, Wyllie PJ, Crewe AV, Isaacson MS, Johnson D. 1970 Petrologic history of the moon inferred from petrography, mineralogy and petrogenesis of Apollo 11 rocks. *Proc. Apollo 11 Lunar Sci. Conf.* **1**, 897–925.

15. Warren PH. 1985 The magma ocean concept and lunar evolution. *Ann. Rev. Earth Planet. Sci.* **13**, 201–240. (doi:10.1146/annurev.ea.13.050185.001221)

16. Wood JA, Dickey JSJ, Marvin UB, Powell BN. 1970 Lunar anorthosites and a geophysical model of the moon. *Proc. Apollo 11 Lunar Sci. Conf.* **1**, 965–988.

17. Donaldson-Hanna KL, Cheek LC, Pieters CM, Mustard JF, Greenhagen BT, Thomas IR, Bowles NE. 2014 Global assessment of pure crystalline plagioclase across the Moon and implications for the evolution of the primary crust. *J. Geophys. Res. Planets* **119**, 1516–1545. (doi:10.1002/2013JE004476)

18. Ohtake M *et al.* 2009 The global distribution of pure anorthosite on the Moon. *Nature* **461**, 236–240. (doi:10.1038/nature08317)

19. Korotev RL, Jolliff BL, Zeigler RA, Gillis JJ, Haskin LA. 2003 Feldspathic lunar meteorites and their implications for compositional remote sensing of the lunar surface and the composition of the lunar crust. *Geochim. Cosmochim. Acta* **67**, 4895–4923. (doi:10.1016/j.gca.2003.08.001)

20. Hawke BR, Peterson CA, Blewett DT, Bussey DBJ, Lucey PG, Taylor GJ, Spudis PD. 2003 Distribution and modes of occurrence of lunar anorthosite. *J. Geophys. Res Planets* **108**, 4.1–4.16. (doi:10.1029/2002JE001890)

21. Besserer J, Nimmo F, Wieczorek, MA, Weber, RC, Kiefer, WS, McGovern, PJ, Andrews-Hanna, JC, Smith, DE, Zuber, MT. 2014 GRAIL gravity constraints on the vertical and lateral density structure of the lunar crust. *Geophys. Res. Lett.* **41**, 5771–5777. (doi:10.1002/2014GL060240)

22. Haskin LA, Lindstrom MM, Salpas PA, Lindstrom D. 1981 On compositional variations among lunar anorthosites. *Proc. Lunar Planet. Sci. Conf.* **12**, 41–66.

23. Morse SA. 1982 Adcumulus growth of anorthosite at the base of the lunar crust. *Proc. Lunar Planet. Sci. Conf.* **13**, A10–A18. (doi:10.1029/JB087iS01p00A10)

24. Ryder G. 1982 Lunar anorthosite 60025, the pertrogenesis of lunar anorthosites, and the bulk composition of the Moon. *Geochem. Cosmochim. Acta* **46**, 1591–1601. (doi:10.1016/0016-7037(82)90316-7)

25. Rai N, van Westrenen W. 2014 Lunar core formation: new constraints from metal-silicate partitioning of siderophile elements. *Earth Planet. Sci. Lett.* **388**, 343–352. (doi:10.1016/j.epsl.2013.12.001)

26. Longhi J. 1980 A model of early lunar differentiation. *Proc. Lunar Planet. Sci. Conf.* **26**, 289–315.

27. Longhi J. 2003 A new view of lunar ferroan anorthosites: postmagma ocean petrogenesis. *J. Geophys. Res.* **108**, 2–1–2–15. (doi:10.1029/2002JE001941)

28. Longhi J. 2006 Petrogenesis of picritic mare magmas: Constraints on the extent of early lunar differentiation. *Geochim. Cosmochim. Acta* **70**, 5919–5934. (doi:10.1016/j.gca.2006.09.023)

29. Taylor SR, Jakes P. 1974 The geochemical evolution of the Moon. *Proc. Lunar Sci. Conf.* **5**, 1287–1305.

30. Snyder GA, Taylor LA, Neal CR. 1992 A chemical model for generating the sources of mare basalts: combined equilibrium and fractional crystallization of the lunar magmasphere. *Geochem. Cosmochim. Acta* **56**, 3809–3823. (doi:10.1016/0016-7037(92)90172-F)

31. Longhi J, Durand SR, Walker D. 2010 The pattern of Ni and Co abundances in lunar olivines. *Geochim. Cosmochim. Acta* **74**, 784–798. (doi:10.1016/j.gca.2009.10.001)

32. Elardo SM, Draper DS, Shearer CK. 2011 Lunar Magma Ocean crystallization revisited: Bulk composition, early cumulate mineralogy, and the source regions of the highlands Mg-suite. *Geochim. Cosmochim. Acta* **75**, 3024–3045. (doi:10.1016/j.gca.2011.02.033)

33. Elkins-Tanton LT, Burgess S, Yin QZ. 2011 The lunar magma ocean: reconciling the solidification process with lunar petrology and geochronology. *Earth Planet. Sci. Lett.* **304**, 326–336. (doi:10.1016/j.epsl.2011.02.004)

34. Piskorz D, Stevenson DJ. 2014 The formation of pure anorthosite on the Moon. *Icarus* **239**, 238–243. (doi:10.1016/j.icarus.2014.06.015)

35. Dygert N, Lin J-F, Marshall EW, Kono Y, Gardner JE. 2017 A low viscosity lunar magma ocean forms a stratified anorthitic flotation crust with mafic poor and rich units. *Geophys. Res. Lett.* **44**, 11 282–11 291. (doi:10.1002/2017GL075703)

36. Meyer J, Elkins-Tanton LT, Wisdom J. 2010 Coupled thermal-orbital evolution of the early Moon. *Icarus* **208**, 1–10. (doi:10.1016/j.icarus.2010.01.029)

37. Chen EMA, Nimmo F. 2013 Tidal dissipation in the lunar magma ocean and its effect on the early evolution of the Earth-Moon system. *Icarus* **275**, 132–142. (doi:10.1016/j.icarus.2016.04.012)

38. Lin Y, Tronche EJ, Steenstra ES, van Westrenen W. 2016 Evidence for an early wet Moon from experimental crystallization of the lunar magma ocean. *Nat. Geosci.* **10**, 14–18. (doi:10.1038/ngeo2845)

39. Lin Y, Tronche EJ, Steenstra ES, van Westrenen W. 2017 Experimental constraints on the solidification of a nominally dry lunar magma ocean. *Earth Planet. Sci. Lett.* **471**, 104–116. (doi:10.1016/j.epsl.2017.04.045)

40. Gaffney *et al.* In preparation. Magmatic evolution I – initial differentiation of the moon.

41. Hui H, Peslier AH, Zhang Y, Neal CR. 2013 Water in lunar anorthosites and evidence for a wet early Moon. *Nat. Geosci.* **6**, 177–180. (doi:10.1038/NGEO1735)

42. Borg LE, Norman M, Nyquist LE, Bogard D, Snyder GA, Taylor L, Lindstrom M. 1999 Isotopic studies of ferroan anorthosite 62 236: a young lunar crustal rock from a light rare-earth-element-depleted source. *Geochem. Cosmochim. Acta* **63**, 2679–2691. (doi:10.1016/S0016-7037(99)00130-1)

43. Borg LE, Shearer CK, Nyquist LE, Norman M. 2002 Isotopic constraints on the origin of lunar ferroan anorthosites. *Proc. Lunar Planet. Sci. Conf.* **33**, 1396.

44. Boyet M, Carlson RW. 2005 142Nd evidence for early (>4.53 Ga) global differentiation of the silicate Earth. *Science* **309**, 576–581. (doi:10.1126/science.1113634)

45. Carlson RW, Lugmair GW. 1988 The age of ferroan anorthosite 60 025: oldest crust on a young Moon? *Earth Planet. Sci. Lett.* **90**, 119–130. (doi:10.1016/0012-821X(88)90095-7)

46. Nyquist LE, Wiesmann H, Bansal B, Shih CY, Keith JE, Harper CL. 1995 ^{146}Sm–^{142}Nd formation interval for the lunar mantle. *Geochim. Cosmochim. Acta* **59**, 2817–2837. (doi:10.1016/0016-7037(95)00175-Y)

47. Nyquist LE, Shih C-Y, Reese YD, Park J, Bogard D, Garrison D, Yamaguchi A. 2010 Lunar crustal history recorded in lunar anorthosites. *Lunar Planet. Sci. Conf.* **41**, 1383.

48. Kleine T, Touboul M, Bourdon B, Nimmo F, Mezger K, Palme H, Jacobsen SB, Yin Q-Z, Halliday A. 2009 Hf-W chronology of the accretion and early evolution of asteroids and terrestrial planets. *Geochim. Cosmochim. Acta* **73**, 5150–5188. (doi:10.1016/j.gca.2008.11.047)

49. Borg LE, Connelly J, Boyet M, Carlson R. 2011 The age of lunar ferroan anorthosite 60 025 with implications for the interpretation of lunar chronology and the magma ocean model. *Proc. Lunar Planet. Sci. Conf.* **42**, 1608.

50. Boyet M, Carlson RW, Borg LE, Horan M. 2015 Sm-Nd systematics of lunar ferroan anorthositic suite rocks: Constraints on lunar crust formation. *Geochim. Cosmochim. Acta* **148**, 203–218. (doi:10.1016/j.gca.2014.09.021)

51. Snape JF, Nemchin AA, Bellucci JJ, Whitehouse MJ, Tartèse R, Barnes JJ, Anand M, Crawford IA, Joy KH. 2016 Lunar basalt chronology, mantle differentiation and implications for determining the age of the Moon. *Earth Planet. Sci. Lett.* **451**, 149–158. (doi:10.1016/j.epsl.2016.07.026)

52. Barboni M, Boehnke P, Keller B, Kohl IE, Schoene B, Young ED, McKeegan KD. 2017 Early formation of the Moon 4.51 billion years ago. *Sci. Adv.* **3**, e1602365. (doi:10.1126/sciadv.1602365)

53. Morbidelli A, Nesvorny D, Laurenz V, Marchi S, Rubie DC, Elkins-Tanton L, Wieczorek M, Jacobson S. 2018 The timeline of the lunar bombardment: revisited. *Icarus* **305**, 262–276. (doi:10.1016/j.icarus.2017.12.046)

54. Hartung JB. 1979 On the global asymmetry of the lunar crust thickness. *LPI Contrib.* **394**, 45.

55. Pernet-Fisher J, Joy K. 2016 The lunar highlands: old crust, new ideas. *Astron. Geo.* **57**, 1.26–1.30.

56. Blichert-Toft J, Gleason JD, Télouk P, Albarède F. 1999 The Lu-Hf isotope geochemistry of shergottites and the evolution of the Martian mantle-crust system. *Earth Planet. Sci. Lett.* **173**, 25–39. (doi:10.1016/S0012-821X(99)00222-8)

57. Borg LE, Connelly JN, Nyquist LE, Shih C-Y, Wiesmann H, Reese Y. 1999 The age of the carbonates in martian meteorite ALH84001. *Science* **286**, 90–94. (doi:10.1126/science.286.5437.90)

58. Bouvier LC *et al.* 2018. Evidence for extremely rapid magma ocean crystallization and crust formation on Mars. *Nature* **558**, 586–589. (doi:10.1038/s41586-018-0222-z)

59. Dauphas N, Pourmand A. 2011 Hf–W–Th evidence for rapid growth of Mars and its status as a planetary embryo. *Nature* **473**, 489–492. (doi:10.1038/nature10077)

60. Senshu H, Kuramoto K, Matsui T. 2002 Thermal evolution of a growing Mars. *J. Geophys. Res.* **107**, 5118. (doi:10.1029/2001JE001819)

61. Ricard Y, Sramek O, Dubuffet F. 2009 A multi-phase model of runaway core-mantle segregation in planetary embryos. *Earth Planet. Sci. Lett.* **284**, 144–150. (doi:10.1016/j.epsl.2009.04.021)

62. Saito H, Kuramoto K. 2017 Formation of a hybrid-type proto-atmosphere on Mars accreting in the solar nebula. *Month. Not. Roy. Astron. Soc.* **475**, 1247–1287.

63. Debaille V, Brandon AD, Yin QZ, Jacobsen B. 2007 Coupled $^{142}Nd/^{143}Nd$ evidence for a protracted magma ocean in Mars. *Nature* **450**, 525–528. (doi:10.1038/nature06317)

64. Humayun M *et al.* 2013 Origin and age of the earliest Martian crust from meteorite NWA 7533. *Nature* **503**, 513–516. (doi:10.1038/nature12764)

65. Nyquist LE, Shih CY, McCubbin FM, Santos AR, Shearer CK, Peng ZX, Burger PV, Agee CB. 2016 Rb-Sr and Sm-Nd isotopic and REE studies of igneous components in the bulk matrix domain of Martian breccia Northwest Africa 7034. *Met. Planet. Sci.* **51**, 483–498. (doi:10.1111/maps.12606)

66. Elkins-Tanton LT, Hess PC, Parmentier EM. 2005 Possible formation of ancient crust on Mars through magma ocean processes. *J. Geophys. Res.* **110**, E12S01. (doi:10.1029/2005JE002480)

67. Elkins-Tanton LT. 2008 Linked magma ocean solidification and atmospheric growth for Earth and Mars. *Earth Planet. Sci. Lett.* **271**, 181–191. (doi:10.1016/j.epsl.2008.03.062)

68. Lebrun T, Massol H, Chassefiere E, Davaille A, Marcq E, Sarda P, Leblanc F, Brandeis G. 2013 Thermal evolution of an early magma ocean in interaction with the atmosphere. *J. Geophys. Res.: Planets* **118**, 1155–1176. (doi:10.1002/jgre.20068)

69. Borg LE, Brennecka GA, Symes SJK. 2016 Accretion timescale and impact history of Mars deduced from the isotopic systematics of martian meteorites. *Geochim. Cosmochim. Acta* **175**, 150–167. (doi:10.1016/j.gca.2015.12.002)

70. Skok JR, Mustard JF, Tornabene LL, Pan C, Rogers D, Murchie SL. 2012 A spectroscopic analysis of Martian crater central peaks: formation of the ancient crust. *J. Geophys. Res.* **117**, E00J18. (doi:10.1029/2012JE004148)

71. Plesa AC, Tosi N, Breuer D. 2014 Can a fractionally crystallized magma ocean explain the thermo-chemical evolution of Mars? *Earth Planet. Sci. Lett.* **403**, 225–235. (doi:10.1016/j.epsl.2014.06.034)

72. Ehlmann BL, Edwards CS. 2014 Mineralogy of the martian surface. *Annu. Rev. Earth Planet. Sci.* **42**, 291–315. (doi:10.1146/annurev-earth-060313-055024)

73. Ramirez R. 2017 A warmer and wetter solution for early Mars and the challenges with transient warming. *Icarus* **297**, 71–82. (doi:10.1016/j.icarus.2017.06.025)

74. Wordsworth R, Kalugina Y, Lokshtanov S, Vigasin A, Ehlmann B, Head J, Sanders C, Wang H. 2013 Transient reducing greenhouse warming on early Mars. *Geophys. Res. Lett.* **44**, 665–671. (doi:10.1002/2016GL071766)

75. Cannon KM, Parman SW, Mustard JF. 2017 Primordial clays on Mars formed beneath a steam supercritical atmosphere. *Nature* **552**, 88–91. (doi:10.1038/nature24657)

76. Sun VZ, Milliken RE. 2015 Ancient and recent clay formation on Mars as revealed from a global survey of hydrous minerals in crater central peaks. *J. Geophys. Res. Planets* **120**, 2293–2332. (doi:10.1002/2015JE004918)

77. Dziewonski AM, Hager BH, O'Connell RJ. 1977 Large-scale heterogeneities in the lower mantle. *J. Geophys. Res.* **82**, 239–255. (doi:10.1029/JB082i002p00239)

78. Su W-J, Woodward RL, Dziewonski AM. 1994 Degree 12 model of shear velocity heterogeneity in the mantle. *J. Geophys. Res.* **99**, 6945–6980. (doi:10.1029/93JB03408)

79. Garnero EJ, McNamara AK. 2008 Structure and dynamics of Earth's lower mantle. *Science* **320**, 626–628. (doi:10.1126/science.1148028)

80. Thorne MS, Garnero EJ. 2004 Inferences on ultralow-velocity zone structure from a global analysis of SPdKS waves. *J. Geophys. Res.* **109**, B08301. (doi:10.1029/2004JB003010)

81. Ishii M, Tromp J. 1999 Constraining large-scale mantle heterogeneity using mantle and inner-core sensitive normal modes. *Phys. Earth Planet. Int.* **146**, 113–124. (doi:10.1016/j.pepi.2003.06.012)

82. Trampert J, Deschamps F, Resovsky J, Yuen D. 2004 Probabilistic tomography maps chemical heterogeneities throughout the lower mantle. *Science* **306**, 853–856. (doi:10.1126/science.1101996)

83. Williams Q, Garnero EJ. 1996 Seismic evidence for partial melt at the base of Earth's mantle. *Science* **273**, 1528–1530. (doi:10.1126/science.273.5281.1528)

84. Lay T, Garnero EJ, Williams Q. 2004 Partial melting in a thermo-chemical boundary layer at the base of the mantle. *Phys. Earth Planet. Inter.* **146**, 441–467. (doi:10.1016/j.pepi.2004.04.004)

85. Rost S, Garnero EJ, Williams Q, Manga M. 2005 Seismological constraints on a possible plume root at the core-mantle boundary. *Nature* **435**, 666–669. (doi:10.1038/nature03620)

86. McNamara AK, Garnero EJ, Rost S. 2010 Tracking deep mantle reservoirs with ultra-low velocity zones. *Earth Planet. Sci. Lett.* **299**, 1–9. (doi:10.1016/j.epsl.2010.07.042)

87. Jellinek AM, Manga M. 2002 The influence of a chemical boundary layer on the fixity, spacing and lifetime of mantle plumes. *Nature* **418**, 760–763. (doi:10.1038/nature00979)

88. McNamara AK, Zhong S. 2005 Thermochemical structures beneath Africa and the Pacific ocean. *Nature* **437**, 1136–1139. (doi:10.1038/nature04066)

89. Becker TW, Kellogg JB, O'Connell R. 1999 Thermal constraints on the survival of primitive blobs in the lower mantle. *Earth Planet. Sci. Lett.* **171**, 351–365. (doi:10.1016/S0012-821X(99)00160-0)

90. Rizo H, Walker RJ, Carlson RW, Touboul M, Horan MF, Puchtel IS, Boyet M, Rosing MT. 2016 Early Earth differentiation investigated through ^{142}Nd, ^{182}W, and highly siderophile element abundances in samples from Isua, Greenland. *Geochim. Cosmochim. Acta* **175**, 319–336. (doi:10.1016/j.gca.2015.12.007)

91. Morino P, Caro G, Reisberg L, Schumacher A. 2017 Chemical stratification in the post-magma ocean Earth inferred from coupled ^{146,147}Sm-^{142,143}Nd systematics in ultramafic rocks of the Saglek block (3.25–3.9 Ga; northern Labrador. Canada). *Earth Planet. Sci. Lett.* **463**, 136–150. (doi:10.1016/j.epsl.2017.01.044)

92. Bouvier A, Boyet M. 2016 Primitive Solar System materials and Earth share a common initial ^{142}Nd abundance. *Nature* **537**, 399–402. (doi:10.1038/nature19351)

93. Kurz MD, Jenkins WJ, Hart SR. 1982 Helium isotopic systematics of oceanic islands and mantle heterogeneity. *Nature* **297**, 43–47. (doi:10.1038/297043a0)

94. Kellogg LH, Wasserburg GJ. 1990 The role of plumes in mantle helium fluxes. *Earth Planet. Sci. Lett.* **99**, 276–289. (doi:10.1016/0012-821X(90)90116-F)

95. Honda R, Mizutani H, Yamamoto T. 1993 Numerical simulation of Earth's core formation. *J. Geophys. Res.* **98**, 2075–2089. (doi:10.1029/92JB02699)

96. Graham DW. 2002 Noble gas isotope geochemistry of midocean ridge and ocean island basalts: characterization of mantle source reservoirs. *Rev. Mineral. Geochem.* **47**, 247–317. (doi:10.2138/rmg.2002.47.8)

97. Tucker JM, Mukhopadhyay S. 2014 Evidence for multiple magma ocean outgassing and atmospheric loss episodes from mantle noble gases. *Earth Planet Sci. Lett.* **393**, 254–265. (doi:10.1016/j.epsl.2014.02.050)

98. Hess P, Parmentier E. 1995 A model for the thermal and chemical evolution of the Moon's interior: implications for the onset of mare volcanism. *Earth Planet. Sci. Lett.* **134**, 501–514. (doi:10.1016/0012-821X(95)00138-3)

99. Ringwood AE, Kesson SE. 1976 A dynamic model for mare basalt petrogenesis. *Proc. Lunar Sci. Conf.* **7**, 1697–1722.

100. Spera FJ. 1992 Lunar magma transport phenomena. *Geochem. Cosmochim. Acta* **56**, 2253–2265. (doi:10.1016/0016-7037(92)90187-N)

101. Debaille V, Brandon AD, O'Neill C, Yin QZ, Jacobsen B. 2009 Early Martian mantle overturn inferred from isotopic composition of nakhlite meteorites. *Nat. Geosci.* **2**, 548–552. (doi:10.1038/ngeo579)

102. Brown SM, Elkins-Tanton ET, Walker RJ. 2014 Effects of magma ocean crystallization and overturn on the development of ^{142}Nd and ^{182}W isotopic heterogeneities in the primordial mantle. *Earth Planet. Sci. Lett.* **408**, 319–330. (doi:10.1016/j.epsl.2014.10.025)

103. Labrosse S, Hernlund JW, Coltice N. 2008 A crystallizing dense magma ocean at the base of the Earth's mantle. *Nature* **450**, 866–869. (doi:10.1038/nature06355)

104. Lee CA, Luffi P, Höink T, Li J, Dasgupta R, Hernlund J. 2010 Upside-down differentiation and generation of a 'primordial' lower mantle. *Nature* **463**, 930–933. (doi:10.1038/nature08824)

105. Tolstikhin I, Hofmann AW. 2005 Early crust on top of the Earth's core. *Phys. Earth Planet. Int.* **148**, 109–130. (doi:10.1016/j.pepi.2004.05.011)

106. Zhang Z, Dorfman SM, Labidi J, Zhang S, Li M, Manga M, Stixrude L, McDonough WF, Williams Q. 2016 Primordial metallic melt in the deep mantle. *Geophys. Res. Lett.* **43**, 3693–3699. (doi:10.1002/2016GL068560)

107. Andrault D *et al.* 2017 Toward a coherent model for the melting behaviour of the deep Earth's mantle. *Phys. Earth Planet. Int.* **265**, 67–81. (doi:10.1016/j.pepi.2017.02.009)

108. Frost DJ, McCammon CA. 2008 The redox state of Earth's mantle. *Ann. Rev. Earth Planet. Sci.* **36**, 389–420. (doi:10.1146/annurev.earth.36.031207.124322)

109. Delano JW. 2001 Redox history of the Earth's interior since ~3900 Ma: implications for prebiotic molecules. *Origins Life Evol. Biosphere* **31**, 311–341. (doi:10.1023/A:1011895600380)

110. Canil D. 1997 Vanadium partitioning and the oxidation state of Archaean komatiite magmas. *Nature* **389**, 842–845. (doi:10.1038/39860)

111. Li ZXA, Lee CTA. 2004 The constancy of upper mantle fO_2 through time inferred from V/Sc ratios in basalts. *Earth Planet. Sci. Lett.* **228**, 483–493. (doi:10.1016/j.epsl.2004.10.006)

112. Nicklas RW, Puchtel IS, Ash RD. 2018 Redox state of the Archean mantle: evidence from V partitioning in 3.5–2.4 Ga komatiites. *Geochim. Cosmochim. Acta* **222**, 447–466. (doi:10.1016/j.gca.2017.11.002)

113. Aulbach S, Stagno V. 2016 Evidence for a reducing Archean ambient mantle and its effects on the carbon cycle. *Geology* **44**, 751–754. (doi:10.1130/G38070.1)

114. Trail D, Watson EB, Tailby ND. 2011 The oxidation state of Hadean magmas and implications for early Earth's atmosphere. *Nature* **480**, 79–82. (doi:10.1038/nature10655)

115. Badro J, Brodholt JP, Piet H, Siebert J, Ryerson FJ. 2015 Core formation and core composition from coupled geochemical and geophysical constraints. *Proc. Nat. Acad. Sci.* **112**, 12 310–12 314. (doi:10.1073/pnas.1505672112)

116. Rubie DC, Frost DJ, Mann U, Asahara Y, Nimmo F, Tsuno K, Kegler P, Holzheid A, Palme H. 2011 Heterogeneous accretion, composition and core-mantle differentiation of the Earth. *Earth Planet. Sci. Lett.* **301**, 31–42. (doi:10.1016/j.epsl.2010.11.030)

117. Rubie DC, Jacobson SA, Morbidelli A, O'Brien DP, Young ED, de Vries J, Nimmo F, Palme H, Frost DJ. 2015 Accretion and differentiation of the terrestrial planets with implications for the compositions of early-formed Solar System bodies and accretion of water. *Icarus* **248**, 89–108. (doi:10.1016/j.icarus.2014.10.015)

118. Sharp ZD, McCubbin FM, Shearer CK. 2013 A hydrogen-based oxidation mechanism relevant to planetary formation. *Earth Planet. Sci. Lett.* **380**, 88–97. (doi:10.1016/j.epsl.2013.08.015)

119. Frost DJ, Liebske C, Langenhorst F, McCammon CA, Tronnes RG, Rubie DC. 2004 Experimental evidence for the existence of iron-rich metal in the Earth's lower mantle. *Nature* **428**, 409–412. (doi:10.1038/nature02413)

120. Wade J, Wood BJ. 2005 Core formation and the oxidation state of the Earth. *Earth Planet. Sci. Lett.* **236**, 78–95. (doi:10.1016/j.epsl.2005.05.017)

121. Fischer RA, Nakajima Y, Campbell AJ, Frost DJ, Harries D, Langenhorst F, Miyajima N, Pollock K, Rubie DC. 2015 High pressure metal-silicate partitioning of Ni, Co, V, Cr, Si, and O. *Geochim. Cosmochim. Acta* **167**, 177–194. (doi:10.1016/j.gca.2015.06.026)

122. Hirschmann M. 2012 Magma ocean influence on early atmosphere mass and composition. *Earth Planet Sci. Lett.* **341–344**, 48–57. (doi:10.1016/j.epsl.2012.06.015)

123. Andrault D, Bolfan-Casanova N, Nigro GL, Bouhifd MA, Garbarino G, Mezouar M. 2011 Solidus and liquidus profiles of chondritic mantle: implication for melting of the Earth across its history. *Earth Planet. Sci. Lett.* **304**, 251–259. (doi:10.1016/j.epsl.2011.02.006)

124. Lange RA, Carmichael ISE. 1989 Ferric-ferrous equilibria in Na_2O-FeO-Fe_2O_3-SiO_2 melts: effects of analytical techniques on derived partial molar volumes. *Geochim. Cosmochim. Acta* **53**, 2195–2204. (doi:10.1016/0016-7037(89)90343-8)

125. Zhang HL, Hirschmann MM, Cottrell E, Withers AC. 2017 Effect of pressure on $Fe^{3+}/\Sigma Fe$ ratio in a mafic magma and consequences for magma ocean redox gradients. *Geochim. Cosmochim. Acta* **204**, 83–103. (doi:10.1016/j.gca.2017.01.023)

126. Kress VC, Carmicheal ISE. 1991 The compressibility of silicate liquids containing Fe_2O_3 and the effect of composition, temperature, oxygen fugacity and pressure on their redox states. *Contrib. Mineral. Petrol.* **108**, 82–92. (doi:10.1007/BF00307328)

127. Komabayashi T. 2015 Thermodynamics of melting relations in the system Fe-FeO at high pressure: implications for oxygen in the Earth's core. *J. Geophys. Res.: Solid Earth* **119**, 4164–4177. (doi:10.1002/2014JB010980)

128. Ricolleau A, Fei Y, Corgne A, Siebert J, Badro J. 2011 Oxygen and silicon contents of Earth's core from high pressure metal-silicate partitioning experiments. *Earth Planet Sci. Lett.* **310**, 409–421. (doi:10.1016/j.epsl.2011.08.004)

129. Kowalski M, Spencer PJ. 1995 Thermodynamic reevaluation of the Cr-O, Fe-O, and Ni-O systems: remodelling of the liquid, BCC, and FCC phases. *Calphad* **19**, 229–243. (doi:10.1016/0364-5916(95)00024-9)

130. Matousek J. 2003 Thermodynamics of iron oxidation in metallurgical slags. *J. Min. Metal Mater. Soc.* **64**, 1314–1320. (doi:10.1007/s11837-012-0461-7)

131. Armstrong, K, Frost, DJ, McCammon, CA, Rubie, DC, Boffa Ballaran, T. 2017 The effect of pressure on iron speciation in silciate melts at a fixed oxygen fugacity: the possibility of a redox profile through a terrestrial magma ocean. *Am. Geophys. Un.* 2017, abstract MR54A-04.

132. Wadhwa M. 2008 Redox conditions on small bodies, the Moon and Mars. *Rev. Mineral. Geochem.* **68**, 493–510. (doi:10.2138/rmg.2008.68.17)

133. Zaranek SE, Parmentier EM. 2004 The onset of convection in fluids with strongly temperature-dependent viscosity cooled from above with implications for planetary lithospheres. *Earth Planet. Sci. Lett.* **224**, 371–386. (doi:10.1016/j.epsl.2004.05.013)

134. Scheinberg A, Elkins-Taton LT, Zhong SJ. 2014 Timescale and morphology of Martian mantle overturn immediately following magma ocean solidification. *J. Geophys. Res. Planets* **119**, 454–467. (doi:10.1002/2013JE004496)

135. Ballmer MD, Lourenco DL, Hirose K, Caracas R, Nomura R. 2017 Reconciling magma-ocean crystallization models with the present-day structure of the Earth's mantle. *Geochem. Geophys. Geosys.* **18**, 2785–2806. (doi:10.1002/2017GC006917)

136. Maurice M, Tosi N, Samuel H, Plesa AC, Hüttig C, Breuer D. 2017 Onset of solid-state mantle convection and mixing during magma ocean solidification. *J. Geophys. Res.* **122**, 577–598. (doi:10.1002/2016JE005250)

137. Tikoo SM, Elkins-Tanton LT. 2016 The fate of water within Earth and super-Earths and implications for plate tectonics. *Phil. Trans. R. Soc. A* **375**, 20150394. (doi:10.1098/rsta.2015.0394)

138. Lenardic A, Crowley JW. 2012 On the notion of well-defined tectonic regimes for terrestrial planets in this solar system and others. *Astrophys. J.* **755**, 132. (doi:10.1088/0004-637X/755/2/132)

139. Weller MB, Lenardic A, O'Neill C. 2015 The effects of internal heating and large scale climate variations on tectonic bi-stability in terrestrial planets. *Earth Planet. Sci. Lett.* **420**, 85–94. (doi:10.1016/j.epsl.2015.03.021)

140. O'Neill C, Lenardic A, Weller M, Moresi L, Quenette S, Zhang S. 2016 A window for plate tectonics in terrestrial planet evolution? *Phys. Earth Planet. Inter.* **255**, 80–92. (doi:10.1016/j.pepi.2016.04.002)

141. Nimmo F, Stevenson DJ. 2000 Influence of early plate tectonics on the thermal evolution and magnetic field of Mars. *J. Geophys. Res.* **105**, 11 969–11 979. (doi:10.1029/1999 JE001216)

142. Debaille V, O'Neill C, Brandon AD, Haenecour P, Yin QZ, Mattielli N, Treiman A. 2013 Stagnant-lid tectonics in early Earth revealed by ^{142}Nd variations in late Archaen rocks. *Earth Planet. Sci. Lett.* **373**, 83–92. (doi:10.1016/j.epsl.2013.04.016)

143. Lourenco DL, Rozel AB, Gerya T, Tackley PJ. 2018 Efficient cooling of rocky planet by intrusive magmatism. *Nat. Geosci.* **11**, 322–327. (doi:10.1038/s41561-018-0094-8)

144. Moore WB, Simon JI, Webb AAG. 2017 Heat-pipe planets. *Earth Planet. Sci. Lett.* **474**, 13–19. (doi:10.1016/j.epsl.2017.06.015)

145. Foley BJ, Bercovici D, Elkins-Tanton LT. 2014 Initiation of plate tectonics from post-magma ocean thermochemical convection. *J. Geophys. Res. Solid Earth* **119**, 8538–8561. (doi:10.1002/2014JB011121)

146. O'Neill C, Marchi S, Zhang S, Bootke W. 2017 Impact-driven subduction on the Hadean Earth. *Nat. Geosci.* **10**, 793–797. (doi:10.1038/ngeo3029)

147. Gerya TV, Stern RJ, Baes M, Sobolev SV, Whattam SA. 2015 Plate tectonics on the Earth triggered by plume-induced subduction initiation. *Nature* **527**, 221–225. (doi:10.1038/nature15752)

148. King C, Olson P. 2011 Heat partitioning in metal-silicate plumes during Earth differentiation. *Earth Planet. Sci. Lett.* **304**, 577–586. (doi:10.1016/j.epsl.2011.02.037)

149. Fleck JR *et al.* 2018 Iron diapirs entrain silicates to the core and initiate thermochemical plumes. *Nat. Comm.* **9**, 71. (doi:10.1038/s41467-017-02503-2)